**Proceedings of the ASME 2016 International Mechanical Engineering Congress and Exposition (IMECE)&
IMECE 2016
November 11 - 17, 2016, Phoenix, AZ, USA**

IMECE2016-67449

COMPRESSIBLE 2D FLOW FIELD INTERACTION OF TWO CONTRA-ROTATING BLADES

Natasha L. Barbely
Aeromechanics Office
NASA Ames Research Center
Moffett Field, CA 94035-0001
Email: Natasha.L.Barbely@nasa.gov

Professor Narayanan M. Komerath
Department of Aerospace Engineering
Georgia Institute of Technology
Atlanta, GA 30332
Email: Komerath@aerospace.gatech.edu

ABSTRACT

The blades of coaxial, contra-rotating rotor systems cross each other in close proximity and at high relative speeds. This crossing event is a potential source of noise and severe blade loads. Effects of compressibility can aggravate the interaction and significantly alter the pressure field signature and phase relationships. A 2-D analysis of this phenomenon is performed by simulating two airfoils passing each other at specified speeds and vertical separation distances. Several test cases spanning a relevant range of Reynolds numbers, angles of attack, and relative Mach number are considered. The Mach number is varied to simulate the radial variation of velocity from the root to tip of a rotor blade to capture the pressure signature, lift, and drag of the airfoils. The velocity and pressure distributions on the airfoils, and in the space between the airfoils are computed before, at, and after airfoil crossing. The variations of lift and drag coefficients through the interaction are captured. The upper airfoil experiences an increase in lift followed by a very sharp drop in lift during the interaction. When relative Mach numbers are transonic, the region of interaction is greatly extended, with shock interactions occurring. The results show the complex nature of the aerodynamic and fluid dynamic impulses generated by blade-blade interactions, with implications to aeroelastic loads and aeroacoustic sources.

NOMENCLATURE

c chord (ft)
c_d coefficient of drag
c_l coefficient of lift
C_p coefficient of pressure
M Mach number
M_{tip} rotor blade tip Mach number
R rotor radius (ft)
r/R dimensionless radial position
V forward flight velocity (ft/s)
V_{tip} rotor blade tip speed (ft/s)
S vertical distance between rotors or airfoils (ft)
α airfoil and blade pitch angle (deg), negative pitch down
μ advance ratio (V/V_{tip})

INTRODUCTION

Coaxial contra-rotating rotor systems are gaining increased interest in civil and military applications. As with all rotorcraft, mitigating noise and overall environmental impact for coaxial rotor systems is important. The increased aerodynamic complexities, such as interactions between the upper and lower rotor, create a challenge for understanding and mitigating noise from these rotor systems. There is limited information on theoretical, analytical, and experimental studies performed on coaxial rotor systems. Coleman [1] surveyed coaxial rotor studies through 1997, starting in the U.S. with the hover test by Taylor in 1950 [2] in the NASA Langley 30' x 60' full-scale wind tunnel. The coax-

ial rotor consisted of two 20-in diameter rotors, with two blades per rotor. The test objective was to visualize the flow through several (single, coaxial, tandem) rotor configurations with and without a ground plane present. Current day analysis validations have relied primarily on the Harrington [3] and Dingeldein [4] large-scale coaxial rotor data from 1952 and 1954, respectively. Ramasamy [5] measured the performance of single, coaxial, tandem, and tiltrotor configurations using untwisted and twisted blade sets. Independent mounting of the two rotors allowed for separate performance measurements of the upper and lower rotors. Ramasamy updated Coleman's survey summary for coaxial rotor hover performance experimental measurements through 2013. More recently, Cameron et al. [6] measured the performance of a single rotor and coaxial rotor system using an 80-in diameter rotor with untwisted blades; the hub loads and blade deformation were also measured. Coaxial rotor measurements in forward flight are even more scarce than hover measurements. The data from the Sikorsky X2 [7] flight test joins the handful of forward flight measurements in the Coleman survey. Computational efforts of simulated coaxial rotors were surveyed by Barbely et al. [8].

One area lacking information is the complex flow field during the crossing of two contra-rotating rotor blades. The overall performance of the lower rotor is affected by the wake of the upper rotor and both rotors are affected by the induced flow. The detailed time-resolved load history on both rotor blades is of great interest, as impulsive loads are expected.

This paper continues the efforts of Barbely et al. [8] [9] where the blade-blade aerodynamic interaction problem was modeled using two airfoils passing each other at specified speeds. In this paper, a range of Mach number, airfoil vertical separation distances and angle of attack are examined. The parameter ranges were selected to include flow conditions of a coaxial rotor system. This simplified 2-D coaxial rotor simulation provides insight into the aerodynamic behavior of this complex flow field.

SIMULATION SPECIFICATIONS

For a coaxial rotor, each rotor operates in the induced flow field produced by the other. As a first step toward understanding this complex, 3D, time-varying flow field in hover, a 2D unsteady simulation of two airfoils traveling in opposite directions was simulated as seen in Fig. 1. The exact location of the airfoils before, at, and after crossing are in the position as seen in Fig. 1, which is carried throughout the paper unless noted.

The initial geometry of the 2D simulation used Harrington Coaxial rotor 1 (HC1) blade tip geometry [3]. The airfoil at the tip of HC1 was a NACA 0012 with a chord length of 0.375. The distance between the upper and lower rotor was 2.33 feet. The tip Mach number tested by Dingeldein for HC1 in forward flight was from 0.47 to 0.52 [4].

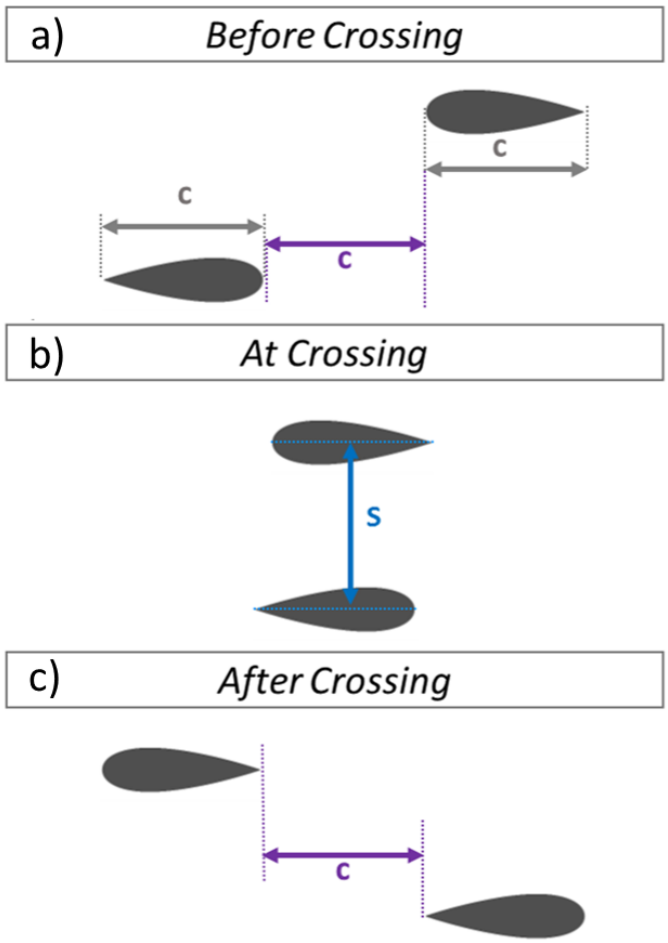

FIGURE 1. 2D OVERFLOW SIMULATION VISUAL OF a) BEFORE, b) AT, AND c) AFTER CROSSING LOCATION.

Test Conditions

Various conditions were explored, including separation distance, angle of attack, and Mach number for a chord length of 0.375 ft (see Table 1) and a NACA 0012 airfoil. For one of the test conditions (Case 15*), a comparison between a NACA 0001 and NACA 0012 was performed. The NACA 0001 airfoil was selected to approximate a thin flat plate. Case 11 flow conditions and geometry were representative of Harrington's coaxial rotor 1 (HC1) in forward flight at an advance ratio of 0.12 at r/R = 1.0 [3]. Case 12 represents the HC1 at an advance ratio of 0.24, or free stream Mach number of 0.52, which was the highest value tested by Dingledien [4]. Atmospheric conditions are provided in Table 2. All calculations in this paper are 2D though can be representative of 3D coaxial rotor at specific r/R locations.

All other cases are outside the flight envelope provided by Dingeldein [4]. Separation distance was varied (0.5, 1.0, 2.33, and 3.5 ft) to understand the sensitivity of proximity (Cases 4, 10, 11, and 14). A speed sweep was performed for Mach numbers of

0.10 through 0.90 (Cases 1 -9). The transonic speeds will create shocks on the airfoil and from there give rise to possible shock-shock interaction from each airfoil passing. The same HC1 geometry and separation distance was used for a higher Mach number simulation of M = 0.90 (Case 13). Angles of attack of 0° and 7° were chosen since they fit inside the HC1 flight envelope performed by Dingeldein [4] (Cases 11 and 15).

TABLE 1. FLIGHT CONDITIONS FOR 2D OVERFLOW SIMULATIONS WITH A CHORD OF 0.375 FT FOR NACA 0012 (*NACA 0001).

Case	S (ft)	S/c	M	$\alpha(^\circ)$	Re
1	0.5	1.33	0.10	7	$2.66\text{x}10^5$
2	0.5	1.33	0.20	7	$5.32\text{x}10^5$
3	0.5	1.33	0.30	7	$7.98\text{x}10^5$
4	0.5	1.33	0.47	7	$1.25\text{x}10^6$
5	0.5	1.33	0.52	7	$1.39\text{x}10^6$
6	0.5	1.33	0.65	7	$1.73\text{x}10^6$
7	0.5	1.33	0.75	7	$1.99\text{x}10^6$
8	0.5	1.33	0.85	7	$2.26\text{x}10^6$
9	0.5	1.33	0.90	7	$2.40\text{x}10^6$
10	1.0	2.67	0.47	7	$1.25\text{x}10^6$
11	2.33	6.22	0.47	7	$1.25\text{x}10^6$
12	2.33	6.22	0.52	7	$1.39\text{x}10^6$
13	2.33	6.22	0.90	7	$2.40\text{x}10^6$
14	3.5	9.34	0.47	7	$1.25\text{x}10^6$
15	0.5	1.33	0.47	0	$1.25\text{x}10^6$
15*	0.5	1.33	0.47	0	$1.25\text{x}10^6$
16	2.33	6.22	0.47	0	$1.25\text{x}10^6$
17	2.33	6.22	0.90	0	$2.40\text{x}10^6$
18	3.5	9.34	0.47	0	$1.25\text{x}10^6$
19	0.5	1.33	0.90	0	$2.40\text{x}10^6$

OVERFLOW

The OVERFLOW flow solver was used to simulate the airfoils. OVERFLOW [10], developed by NASA, is a compressible Reynolds Averaged Navier-Stokes CFD analysis tool that uses overset grids. For time-resolved calculations, OVERFLOW computes not only spatial distortions due to Mach number effects, but also temporal effects due to the finite propagation time of pressure disturbances.

TABLE 2. ATMOSPHERIC CONDITIONS FOR 2D OVERFLOW SIMULATIONS.

Variable	Value	Units
pressure	2118.17	(lbf/ft^2)
viscosity	$3.737\text{x}10^{-7}$	(slug/(s-ft))
density	0.002377	(slug/ft^3)
temperature	518.7	(R°)
speed of sound	1116.46	(ft/s)

All OVERFLOW calculations used the following numerical schemes: ARC3D diagonalized Beam-Warming scalar pentadiagonal scheme for the left hand side and central difference Euler terms for the right hand side. The spacing of off-body grids was set to ds = 0.20 chord lengths. For both the upper and lower airfoils, the number of grid points around each airfoil is 253 and 65 in the normal direction. The spacing between the surface of the airfoil and first grid point was 1.0 x 10-6 chord lengths and the distance to the far-field boundaries was 400 chord lengths.

RESULTS

An isolated NACA 0012 airfoil at $\alpha = 7^\circ$ was analyzed first for subsonic to transonic Mach numbers. The effect of including a second airfoil on the flow field was then explored for the cases shown Table 1.

Isolated airfoil

A Mach number sweep simulation was performed from 0.10 to 0.90 for a single NACA 0012 airfoil at $\alpha = 7^\circ$. Figure 2 shows the variation with Mach number for c_l and c_d. Figures 3 and 4 show $\Delta\ C_p$ verses non-dimensional chord (x/c) for the same Mach number range.

An increase in c_d with increasing Mach number was observed, which was expected due to shocks and viscous forces increasing with Mach number [11]. From Mach 0.10 to 0.52, an increase in c_l was observed. From Mach 0.52 to 0.85 a decease in c_l was seen (Fig. 2). The same conclusion for an an increase in c_l from Mach 0.10 to 0.52 is seen in Fig. 3. Figure 3 shows that the increase in c_l was due to the increase in $\Delta\ C_p$ on the front half (x/c $<$ 0.50) of the airfoil. After Mach 0.52, a decrease in c_l was observed because flow was supersonic over most of the lower surface and decelerated to subsonic speed through a shock wave at the trailing edge. Thus, the lower surface pressures are lower than before Mach 0.52. The formation of a shock wave on the upper surface became more apparent from the $\Delta\ C_p$ behavior,

as seen in Fig. 4 in comparison to Fig. 3. As the Mach number increased further to 0.90, c_l increased due to the upper surface shock wave moving to the trailing edge, where the local Mach number was supersonic for most of the airfoil [11].

The location of the shock wave can be determined from Fig. 4. For example, at Mach 0.85 and 0.90, the shock was at x/c = 0.45 and 0.97, respectively.

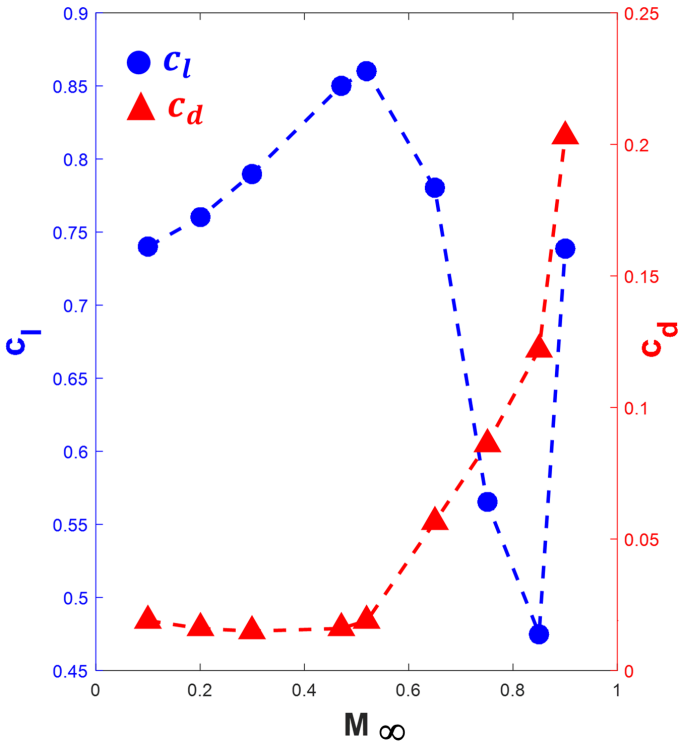

FIGURE 2. MACH NUMBER VARIATION FOR c_l AND c_d FOR A NACA 0012 AIRFOIL AT $\alpha = 7°$.

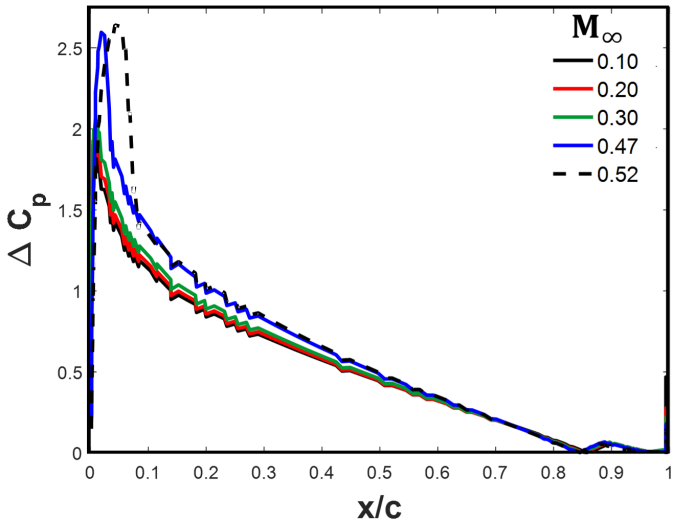

FIGURE 3. MACH NUMBER VARIATION (M = 0.10, 0.20, 0.30, 0.47, AND 0.52) OF ΔC_P FOR A NACA 0012 AIRFOIL AT $\alpha = 7°$.

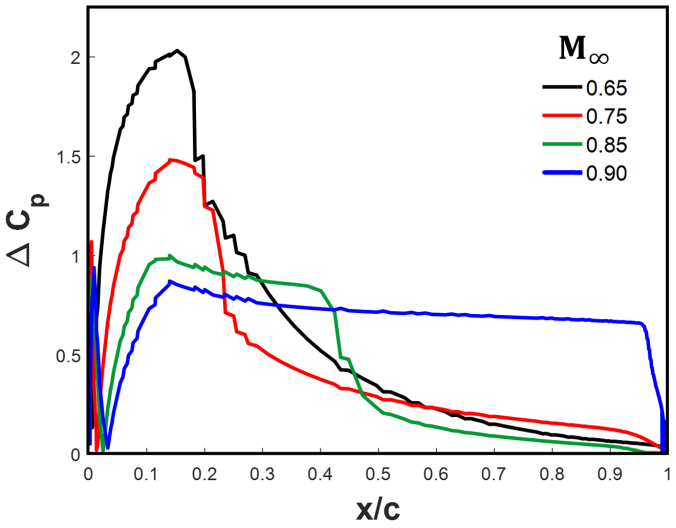

FIGURE 4. MACH NUMBER VARIATION (M = 0.65, 0.75, 0.85, AND 0.90) OF ΔC_P FOR A NACA 0012 AIRFOIL AT $\alpha = 7°$.

Two airfoils crossing: separation distance variation

Two blades passing in close proximity can cause strong compressibility effects impacting noise generation. Figure 5 compares c_l and c_d over time for NACA 0012 airfoils at M = 0.47, $\alpha = 7°$, and a separation distance of S = 0.5 and 3.5 ft (Cases 4 and 14). For both separation distances, the lift produced by both airfoils increases prior to overlap and then decreases after overlap. At a separation distance of 0.5 ft, the variation in c_l was greater compared to the 3.5 ft separation distance. Figure 5 b) shows the c_d over time at a separation distance of 0.5 and 3.5 ft. A 0.003 decrease in c_d occurs before overlap and a 0.002 increase in c_d occurs after overlap for the upper and lower airfoil. The relatively small change in lift and drag at S = 3.5 ft was due to the fact that the two airfoils were further away from the disturbance caused by the other airfoil.

Figure 6 compares c_l and c_d over time for NACA 0012 airfoils at M = 0.47, $\alpha = 0°$ and a separation distance variation of S = 0.5 and 3.5 ft (Cases 15 and 18). The aerodynamic flow field at S = 3.5 ft experiences a minimal change for each airfoil as they approach each other. Since the airfoils are at $\alpha = 0°$ compared to $\alpha = 7°$, as seen in Fig. 5 a), there is less change in the aerodynamics and flow field variation. At S = 0.5 ft, each airfoil's flow field is much more strongly influenced by the other airfoil's surrounding flow field compared to S = 3.5 ft. At a separation

distance of 0.5 ft, as the two airfoils approach each other, the upper airfoil produces more lift, while the lower airfoil produces less lift as seen in Fig. 6 a). After the overlap, the upper airfoil sees a sharp increase in lift followed by small increase and decrease, while the lower airfoil undergoes the same behavior, but opposite in sign. Figure 6 b) reveals no change in c_d for S = 3.5 ft, but a small change in c_d for S = 0.5 ft. At S = 0.5 ft, as the two airfoils are approaching each other, a sharp decrease in drag was observed, followed by a sharp increase in drag at overlap. As expected for a symmetrical airfoil at $\alpha = 0^\circ$, the c_l behavior of the upper and lower NACA 0012 airfoils are anti-symmetric.

The pressure coefficient C_p distribution is shown in Fig. 7 for NACA 0012 airfoils at M = 0.47, $\alpha = 7^\circ$ for separation distances of S = 0.5, 1.0, 2.33, and 3.50 ft (Cases 4, 10, 11, and 14). Figure 7 shows the C_p distribution before, at, and after the crossing as illustrated in Fig. 1. Changes in separation distance are noted near the leading edge. Before the airfoils cross (Figs. 7 a), 7 b)), the suction peak moves closer to the leading edge as separation distance increases. During crossing, the lower airfoil (Figs. 7 d)) experiences a decrease in pressure on the lower surface as separation distance decreases, giving rise to a decrease in lift as seen in Fig. 5 a) at time of overlap. After the airfoils cross (Figs. 7 e), 7 f)), the suction peak moves slightly toward the trailing edge with increasing separation distance, opposite of Figs. 7 g) and 7 h).

Two airfoils crossing: Mach number variation

With increasing Mach number, the disturbance in flow field are propagated further away from the source, resulting in larger fluctuations at the time of overlap for high Mach numbers. Figure 8 compares c_l and c_d over time for NACA 0012 airfoils at a separation distance of 2.33 ft, angle of attack of 7°, and M = 0.47 and 0.90 (Cases 11 and 13). Figure 8 a) reveals lower lift produced at transonic speeds, but as the airfoils move closer to each other, the aerodynamic behavior at Mach 0.47 and 0.90 differ. At Mach 0.47, as the airfoils move closer to each other, the lower airfoil sees a larger increase in lift at an earlier time compared to the upper airfoil. After the time of crossing, the upper airfoil sees a greater decrease in lift compared to the lower airfoil. At Mach 0.90 the trends for the upper and lower airfoils are reversed. As the airfoils move closer to each other, the upper airfoil produces a larger increase in lift earlier compared to the lower airfoil. After the time of crossing, the upper airfoil produces a greater decrease in lift compared to the lower airfoil. At Mach 0.47, drag on each of the airfoils changes less drastically while approaching each other compared to Mach 0.90 in Fig. 8 b). For Mach 0.90, as the airfoils approach each other the drag increases slightly and then decreases at time of overlap. During overlap, the drag decreases more for the upper airfoil than the lower airfoil. The upper surface shock on the lower airfoil was stronger than the lower surface shock on the upper airfoil, therefore the upper airfoil enters a larger change in aerodynamic flow field compared to the lower airfoil.

C_p distribution is shown in Fig. 9 for NACA 0012 airfoils separated by 2.33 ft, angle of attack of 7°, and M = 0.47, 0.52, and 0.90 (Cases 11, 12, and 13) before, at, and after the crossing. At Mach 0.90, the C_p distribution reveals the presence of a shock towards the trailing edge of both airfoils [11].

Figure 10 compares c_l and c_d for NACA 0012 airfoils at a separation distance of 0.50 ft, angle of attack of 7°, and a Mach number variation. The Mach numbers 0.10, 0.20, 0.30, 0.47 and 0.52 are representative of a rotor blade r/R location of 0.1, 0.2, 0.3, 0.5, and 0.6 respectively. The change in c_l when the airfoils are in proximity to one another changes as Mach number increases: the higher the Mach number, the greater change in c_l and c_d for both the upper and lower airfoil at overlap.

Figure 11 compares c_l and c_d for NACA 0012 airfoils at a separation distance of 0.50 ft, angle of attack of 7°, and a Mach number variation of M = 0.65, 0.75, 0.85, and 0.90, corresponding to an r/R location of 0.7, 0.8, 0.9, and 1.0 respectively. As Mach number increases, the more c_l and c_d increase at time of overlap for both the upper and lower airfoil.

A series of ΔC_p distributions are stacked together to represent rotor blade loading from root to tip, where M_{tip} = 0.90, S = 0.50 ft, and $\alpha = 7^\circ$ (see Fig. 12, Cases 1-9). Figures. 12 a, b, and c represent upper airfoil before crossing (*75 chord lengths away), upper airfoil at crossing, and lower airfoil at crossing, respectively. A decrease in ΔC_p was seen at the time of overlap for both the upper and lower airfoil, which corresponded to a decrease in lift, as seen in Figs. 10 and 11. Multiple curved ridges and valleys were seen across the span of the blade at the time of overlap, which revealed how the aerodynamic performance of the upper and lower airfoil was sensitive to Mach number variation.

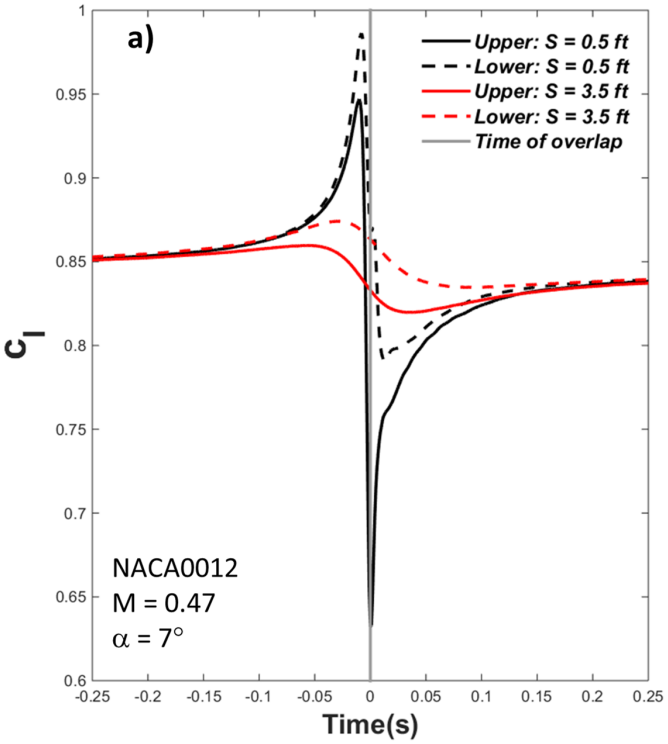

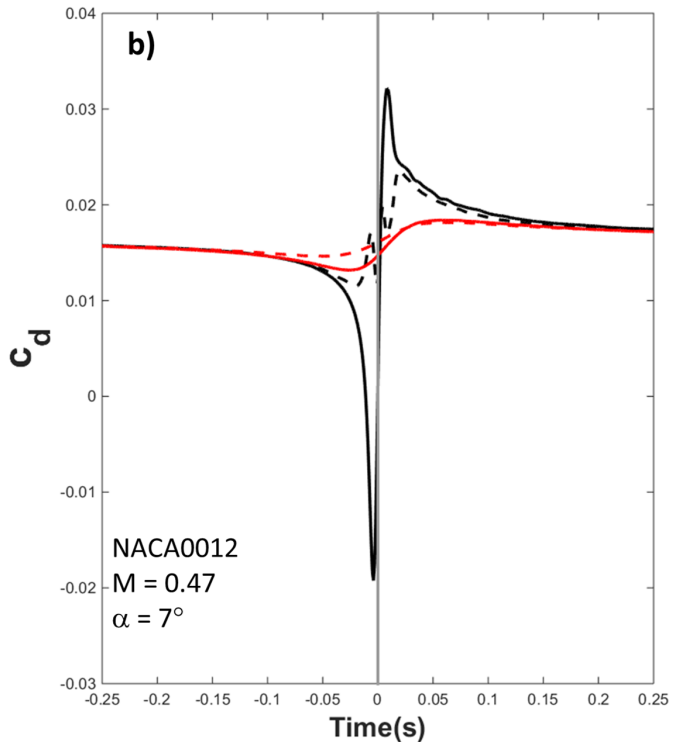

FIGURE 5. NACA 0012 AIRFOILS AT M = 0.47, $\alpha = 7°$, AND S = 0.5 AND 3.50 FOR a) c_l AND b) c_d.

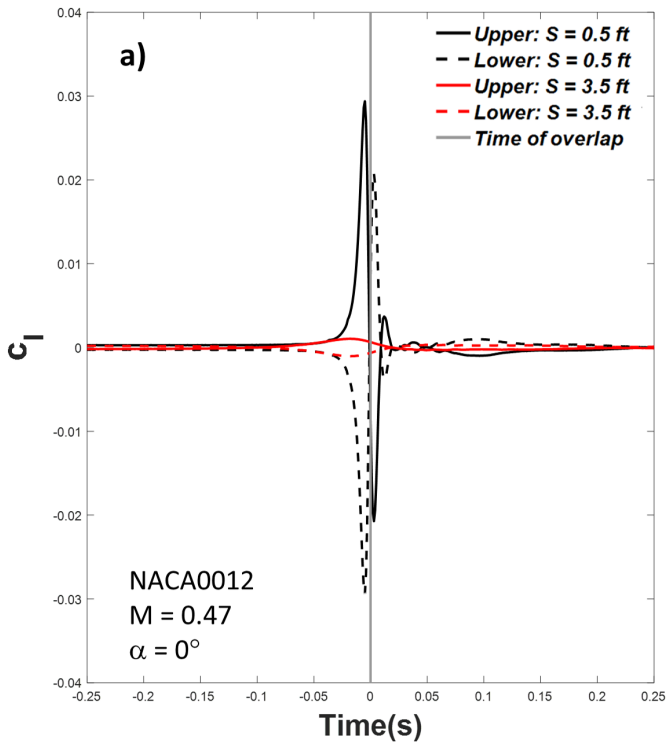

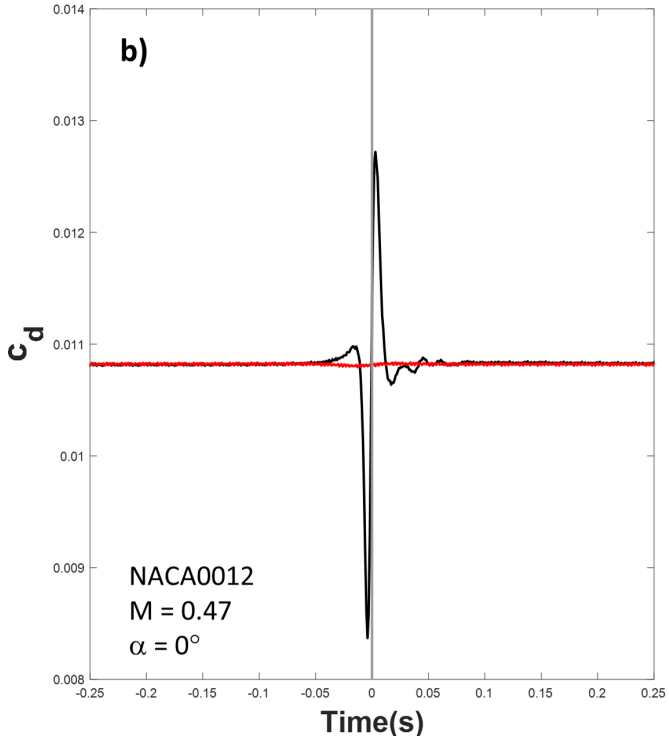

FIGURE 6. NACA 0012 AIRFOILS AT M = 0.47, $\alpha = 0°$, AND S = 0.5 AND 3.50 FOR a) c_l AND b) c_d.

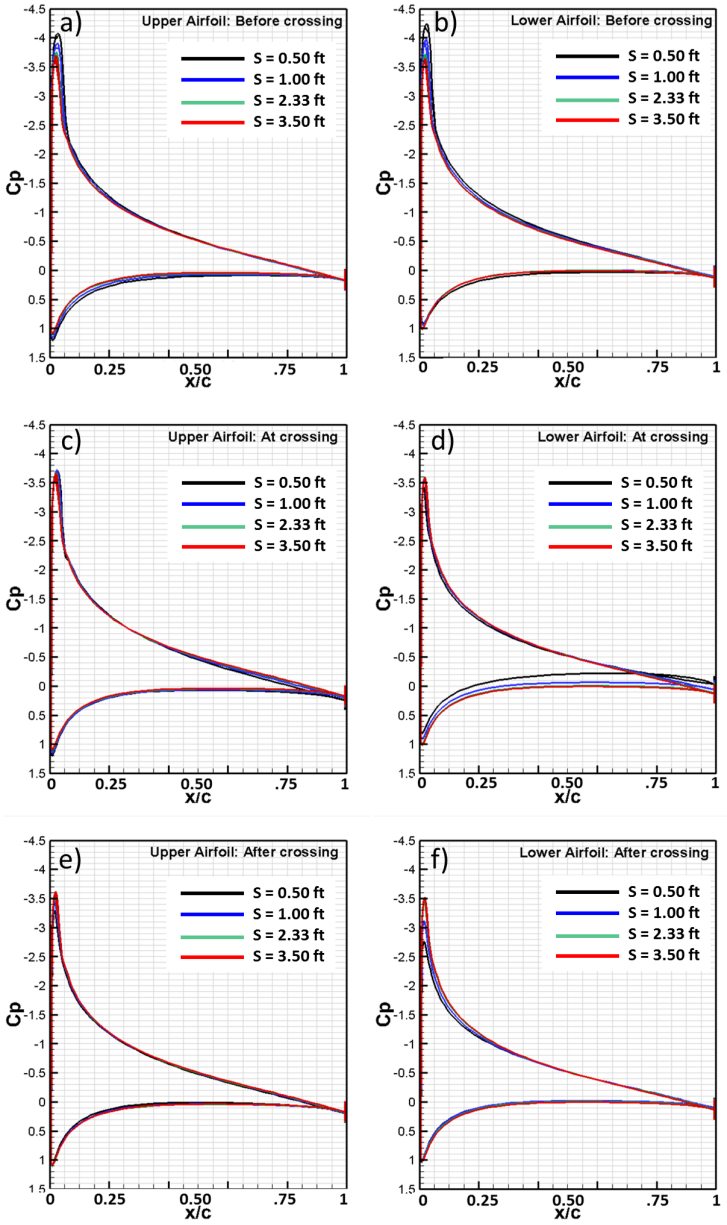

FIGURE 7. C_P DISTRIBUTION FOR NACA 0012 AIRFOILS AT M = 0.47, α = 7°, AND S = 0.5, 1.0, 2.33, AND 3.50 FT FOR UPPER AIRFOIL a) BEFORE, c) AT, AND e) AFTER AND LOWER AIRFOIL b) BEFORE, d) AT, AND f) AFTER CROSSING.

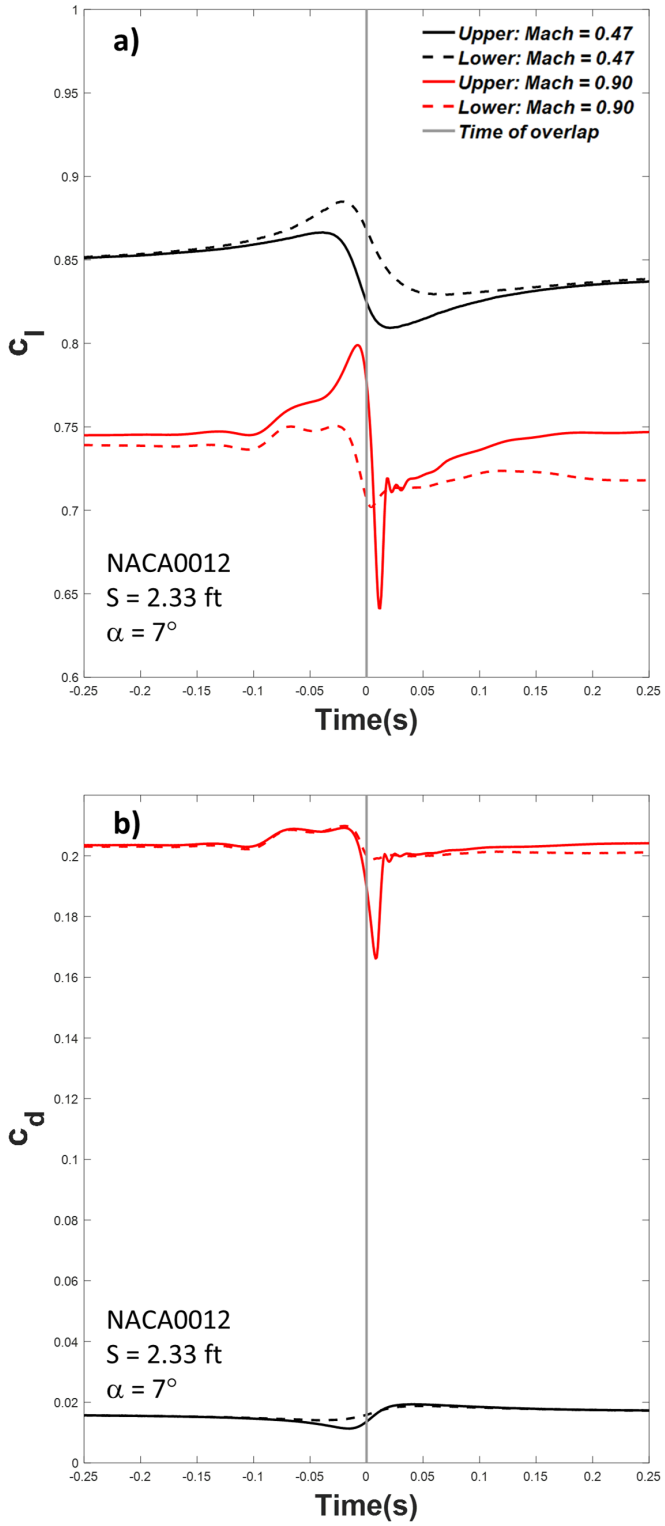

FIGURE 8. NACA 0012 AIRFOILS AT S = 2.33 FT, α = 7°, AND M = 0.47 AND 0.90 FOR a) c_l AND b) c_d.

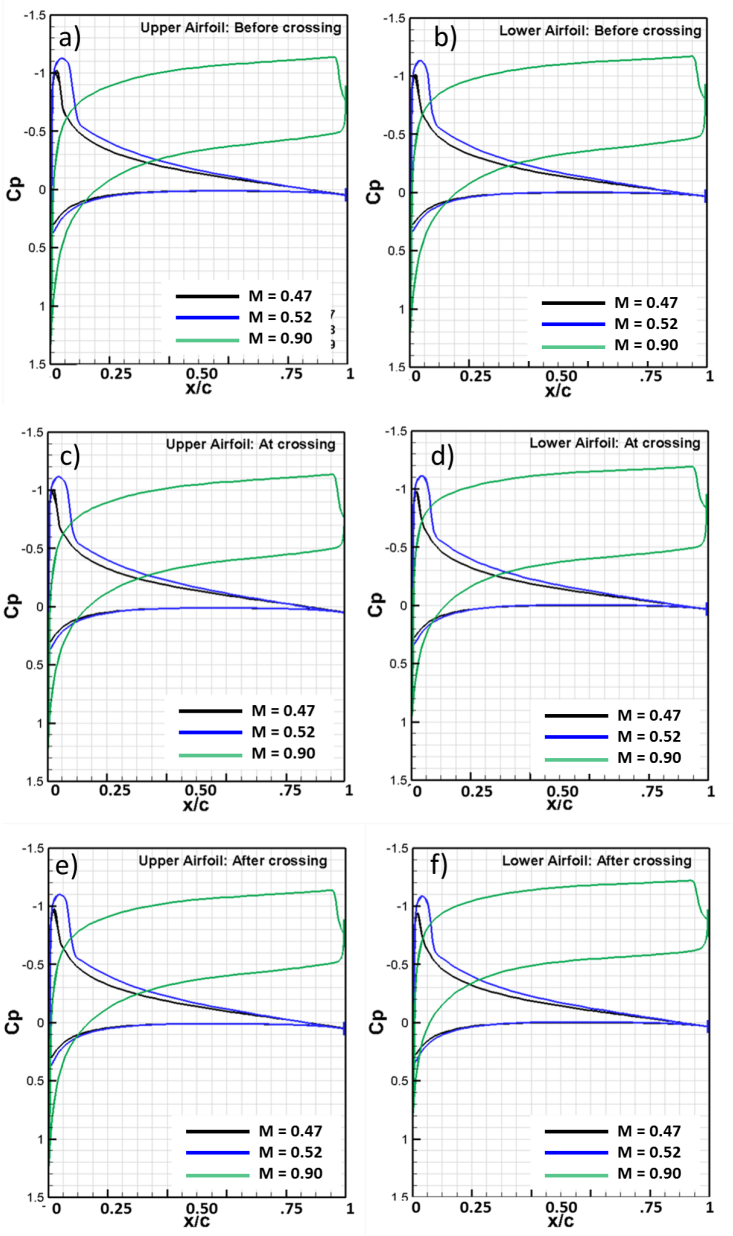

FIGURE 9. C_P DISTRIBUTION FOR NACA 0012 AIRFOILS AT S = 2.33 FT, $\alpha = 7^\circ$, AND M = 0.47, 0.52, AND 0.90 FOR UPPER AIRFOIL a) BEFORE, c) AT, AND e) AFTER AND LOWER AIRFOIL b) BEFORE, d) AT, AND f) AFTER CROSSING.

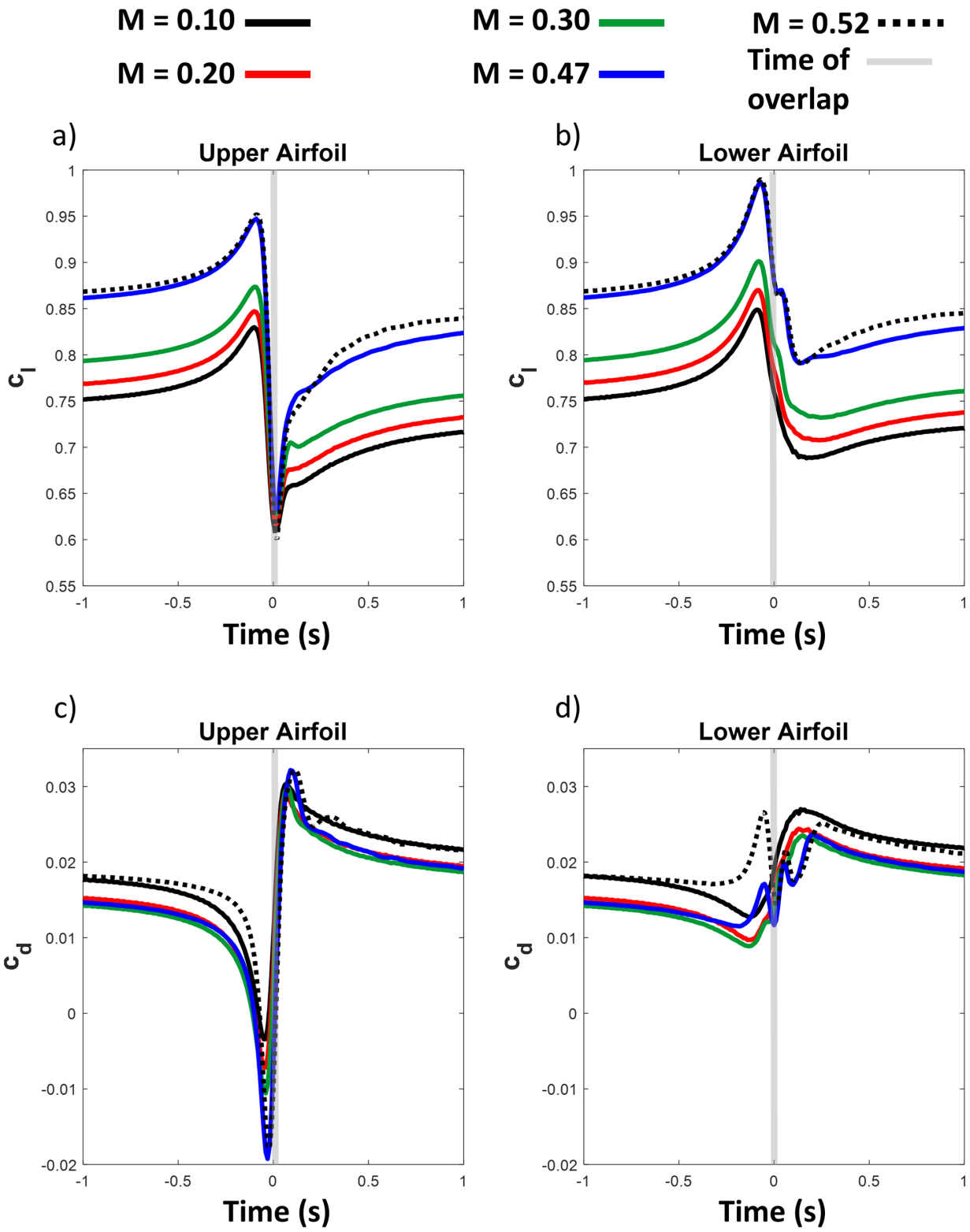

FIGURE 10. MACH NUMBER VARIATION OF M = 0.10, 0.20, 0.30, 0.47, AND 0.52 FOR c_l AND c_d FOR NACA 0012 AIRFOILS AT $\alpha = 7°$, AND S = 0.5 FT FOR a), b) UPPER AND b), d) LOWER AIRFOIL.

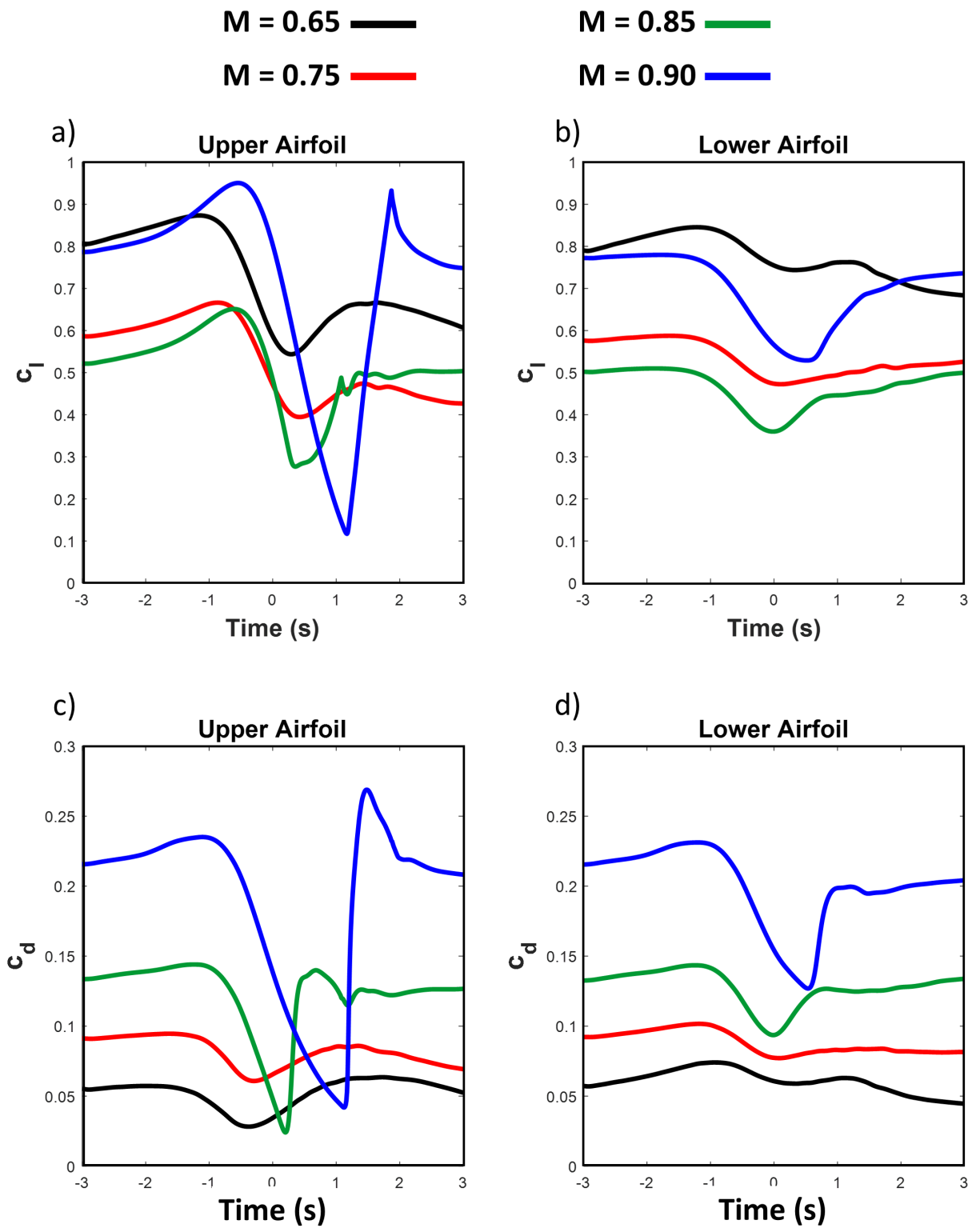

FIGURE 11. MACH NUMBER VARIATION OF M = 0.65, 0.75, 0.85, AND 0.90 FOR c_l AND c_d FOR NACA 0012 AIRFOILS AT $\alpha = 7°$, AND S = 0.5 FT FOR a), c) UPPER AND b), d) LOWER AIRFOIL.

Two airfoils crossing: angle of attack variation

Figure 13 compares C_p before, at, and after the crossing for airfoils separated by 2.33 ft, at M = 0.47, and at an angles of attack of 7° and 0° (Cases 11 and 15). Figures 13 a, c, and e, show that at an angle of attack of 7° for the upper airfoil, the upper surface C_p decreases at the time of overlap compared to before overlap and then increases after overlap compared to at time of overlap. Figures 13 b), d), and f) at an angle of attack of 7°, show the C_p for the lower airfoil, where C_p continues to decreases from before, at, and after overlap on the upper surface of the airfoil. In Fig. 13, no visible difference in C_p was seen for $\alpha = 0°$.

Figures 14 compares c_l and c_d over time for NACA 0012 airfoils separated by 2.33 ft, at M = 0.47, and at an angle of attack of 7° and 0°. As shown in Fig. 13 for $\alpha = 7°$, at the time of overlap the upper and lower airfoil produce a decrease in lift as seen in Fig. 14 a). At $\alpha = 0°$, the c_l of the upper airfoil increases while the lower airfoil decreases before the overlap, then the opposite occurs at time of overlap, which was not discernible in Fig. 13. Figure 14 b) shows a small (less than 0.005) change in drag at $\alpha = 0°$ for both the upper and lower airfoil. At an angle of attack of 7°, the upper airfoil sees a sharp decrease in drag before crossing, followed by a sharp increase in drag. The lower airfoil sees a small decrease then an increase in drag before crossing. After crossing, the lower airfoil sees an increase followed by a decrease in drag.

Two airfoils crossing: NACA 0001 and NACA 0012 airfoils

A pair of NACA 0001 airfoils at M = 0.47, $\alpha = 0°$, and S = 0.5 ft was compared with a pair of NACA 0012 airfoils under similar conditions, (see Fig. 15). For NACA 0001, as the airfoils approached each other, no discernible difference in c_l and c_d are seen when compared to a NACA 0012. Further investigation into the flow field revealed small pressure fluctuations around each NACA 0001 with little or no flow field interaction between the upper and lower airfoil at time of overlap, as was expected for flat plates.

Flow field pressure distribution of two airfoils

The pressure fields predicted by OVERFLOW for four different cases are shown in Fig. 16 when the airfoils are crossing, and separated by 2.33 ft. Figures 16 a) and b) show the pressure field for angles of attack of 7° and 0°, respectively, at Mach 0.47 (Case 11 and 16). Figures 16 a) and b) reveal only a small interference between pressure fields. Figure 16 b) reveals a symmetrical pressure field below and above each airfoil, while Fig. 16 a) reveals asymmetry, because lift was produced. Figures 16 c) and d) show the pressure field for angles of attack of 7° and 0°, respectively, at Mach 0.90 (Case 13 and 17). For both Figs. 16 c) and d), the flow field surrounding each airfoil was affected by the presence of the other airfoil, with Fig. 16 c) showing a large interaction between flow fields.

The interaction between the upper and lower airfoil was further examined in Fig. 17 for two NACA 0012 airfoils at M = 0.90, S = 0.5 ft, and $\alpha = 0°$ (Case 19). As previously mentioned, the transonic speed of Mach 0.90 will create shocks on the airfoil and give rise to possible shock-shock interaction from each airfoil passing in close proximity. Though M = 0.90 and S = 0.5 ft are unrealistic conditions for a coaxial rotor system, the aerodynamic interactions are interesting to analyze as an extreme case. Figure 17 shows the flow field Mach number distribution, where the presence of shocks are formed at the trailing edge of each airfoil.

CONCLUDING REMARKS

To simplify the complex 3D problem of a coaxial rotor flow field, a 2D unsteady simulation of two airfoils traveling in opposite directions was performed using OVERFLOW. The effects of varying flight conditions, geometry, and airfoil separation distance on the aerodynamic flow field characteristics was analyzed. The computed OVERFLOW results show the expected features for a single NACA 0012 airfoil over a range of Mach numbers at $\alpha = 7°$. As the Mach number increases, a shock forms and moves towards the trailing edge of the airfoil.

For two airfoils moving past each other, the sharp changes in lift and drag, occurring during airfoil interaction, provide a glimpse into the implications for blade vibratory loads and noise mitigation. As the separation distance decreases, the flow field becomes more complex as each airfoil operates in the flow field of the other. The present computations focus on separation distances that are as small as they are likely to be in counter-rotating rotor applications. As the two airfoils approach each other, an increase in lift was seen for the upper and lower airfoil, and a decrease after the period of overlap. As the angle of attack was increased, the interaction between the flow fields becomes stronger. Compared to the NACA 0012, the NACA 0001 showed no discernible difference for both aerodynamic and flow field characteristics at the time of airfoil crossing.

Increasing the Mach number also gave rise to increased flow field disturbances as the airfoils approach each other. The Mach number was varied to simulate the radial variation of velocity from the root to tip of a rotor blade. The high Mach cases (above M = 0.52) were studied for curiosity, although coaxial rotorcraft are not expected to push into that regime in the near future. As the Mach number was varied, the pressure distribution has a delayed influence due to the time lag caused by sound propagation time, which becomes significant to the interaction. This complex ΔC_p radial distribution reveals the aerodynamic performance of the upper and lower airfoil is very dependent on the Mach number.

ACKNOWLEDGEMENTS

The authors would like to thank the U. S. Army Aviation Development Directorate (ADD), with personal thanks to Dr. William Warmbrodt (NASA), Dr. Gloria Yamauchi (NASA) and Mr. Ethan Romander (NASA). Dr. Kenneth Brentner (The Pennsylvania State University) is also acknowledged for his support and advice in the research.

REFERENCES

[1] Coleman, C. P., 1997. A survey of theoretical and experimental coaxial rotor aerodynamic research. NASA TP-3675, NASA, March.

[2] Taylor, M. K., 1950. A balsa-dust technique for air-flow visualization and its application to flow through model helicopter rotors in static thrust. NACA TN- 2220, NACA, November.

[3] Harrington, R. D., 1951. Full-scale-tunnel investigation of the static-thrust performance of a coaxial helicopter rotor. NACA TN- 2318, NACA, March.

[4] Dingeldein, R. C., 1954. Wind-tunnel studies of the performance of multirotor configurations. NACA TN- 3236, NACA, August.

[5] Ramasamy, M., 2013. "Measurements comparing hover performance of single, coaxial, tandem, and tilt-rotor configurations". In American Helicopter Society 69th Annual Forum.

[6] Cameron, C. G., Uehara, D., and Sirohi, J., 2015. "Transient hub loads and blade deformation of a mach-scale coaxial rotor in hover". In AIAA Science and Technology Forum and Exposition, SciTech.

[7] Walsh, D., Weiner, S., Arifian, K., Lawrence, T., Wilson, M., Millott, T., and Blackwell, R., 2011. "High airspeed testing of the sikorsky x2 technology demonstrator". In American Helicopter Society 67th Annual Forum.

[8] Barbely, N. L., Komerath, N. M., and Novak, L. A., 2016. "A study of coaxial rotor performance and flow field characteristics". In American Helicopter Society Technical Meeting on Aeromechanics Design for Vertical Lift.

[9] Barbely, N., and Komerath, N., 2016. "Coaxial rotor flow phenomena in forward flight". In International Powered Lift Conference (IPLC) and SAE Aerospace Systems and Technology Conference.

[10] Nichols, R., and Buning, P., 2010. "Users manual for overflow 2.2". *NASA Langley Research Center, Hampton, VA, Aug*.

[11] Bertin, J. J., and Smith, M. L., 1998. *Aerodynamics for Engineers*. Prentice-Hall.

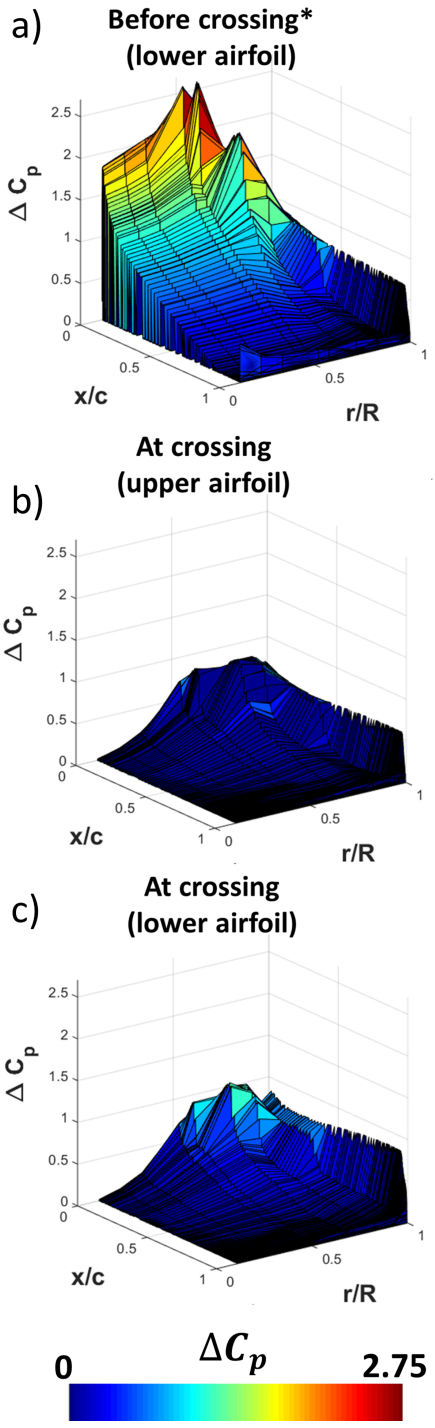

FIGURE 12. ΔC_P RADIAL DISTRIBUTION (ROOT TO TIP) FOR NACA 0012 AIRFOILS AT $M_{tip} = 0.90$, S = 0.50 ft, $\alpha = 7^\circ$ a) LOWER AIRFOIL BEFORE CROSSING (*75 CHORD LENGTHS AWAY), b) UPPER AIRFOIL AT CROSSING, AND c) LOWER AIRFOIL AT CROSSING.

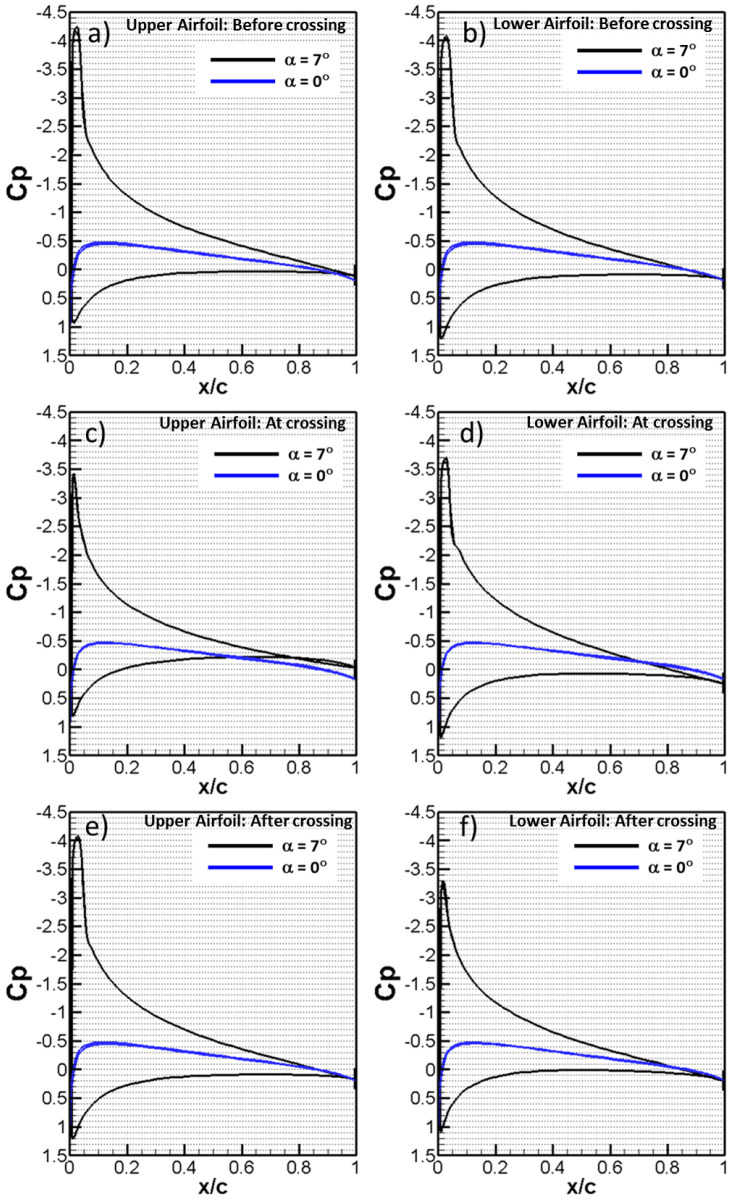

FIGURE 13. C_P DISTRIBUTION FOR NACA 0012 AIRFOILS AT M = 0.47, S = 2.33 FT AND $\alpha = 0°$ AND 7° FOR UPPER AIRFOIL a) BEFORE, c) AT, AND e) AFTER AND LOWER AIRFOIL b) BEFORE, d) AT, AND f) AFTER CROSSING.

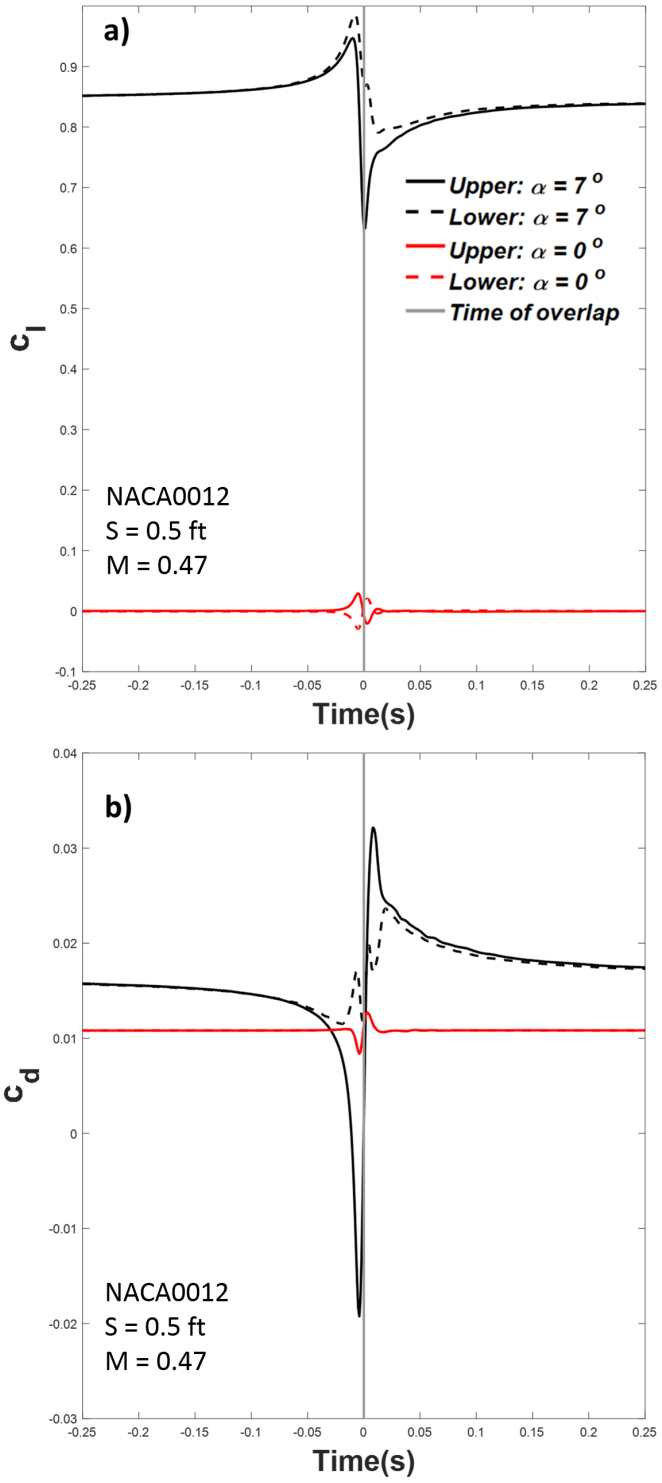

FIGURE 14. NACA 0012 AIRFOILS AT M = 0.47, S = 0.5 FT, AND $\alpha = 7°$ AND 0° FOR a) c_l AND b) c_d.

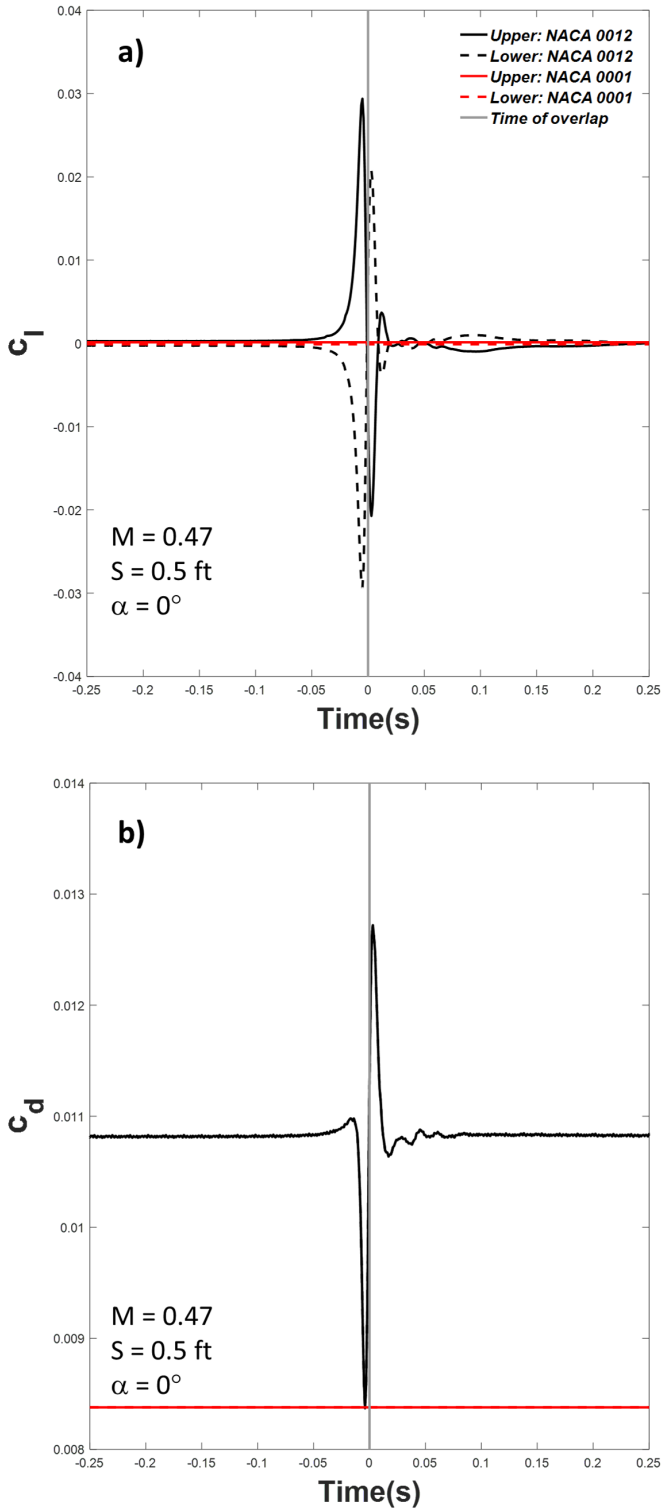

FIGURE 15. c_l AND c_d FOR NACA 0001 AND NACA 0012 AIRFOILS AT M = 0.47, $\alpha = 0°$, AND S = 0.5 FT.

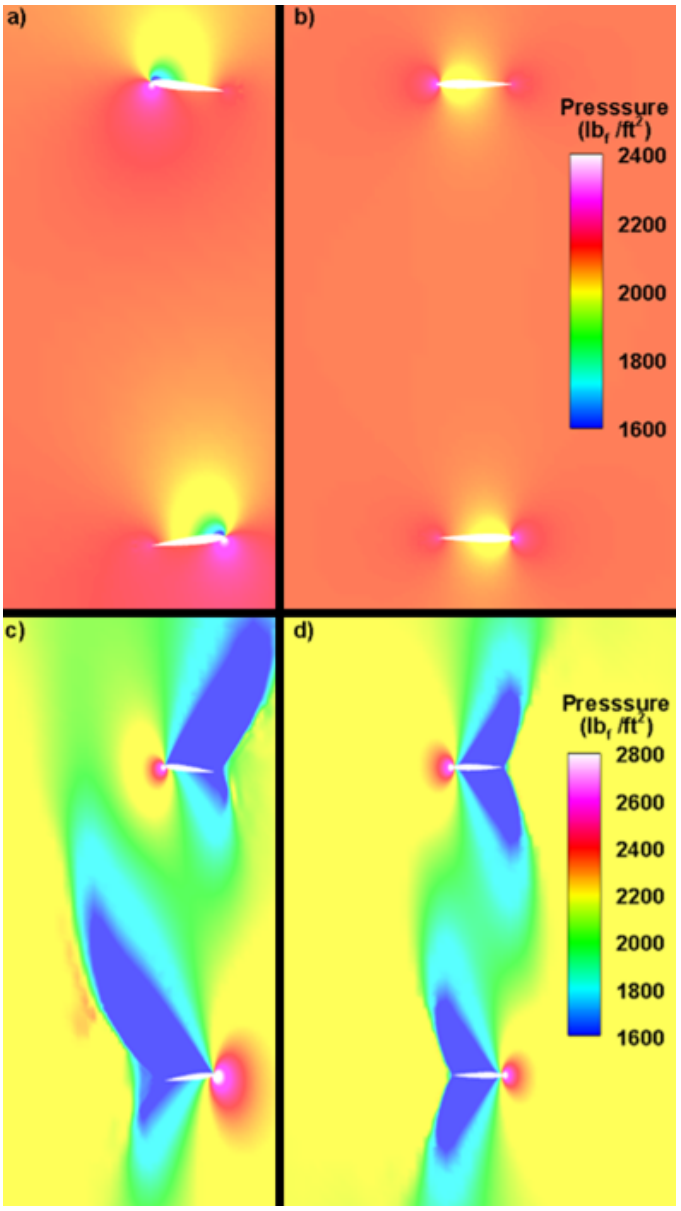

FIGURE 16. FLOW FIELD PRESSURE DISTRIBUTION CALCULATIONS AT CROSSING FOR NACA 0012 AIRFOILS AT S = 2.33 FT AT a) M = 0.47, $\alpha = 7°$, b) M = 0.47, $\alpha = 0°$, c) M = 0.90, $\alpha = 7°$, AND d) M = 0.90, $\alpha = 0°$.

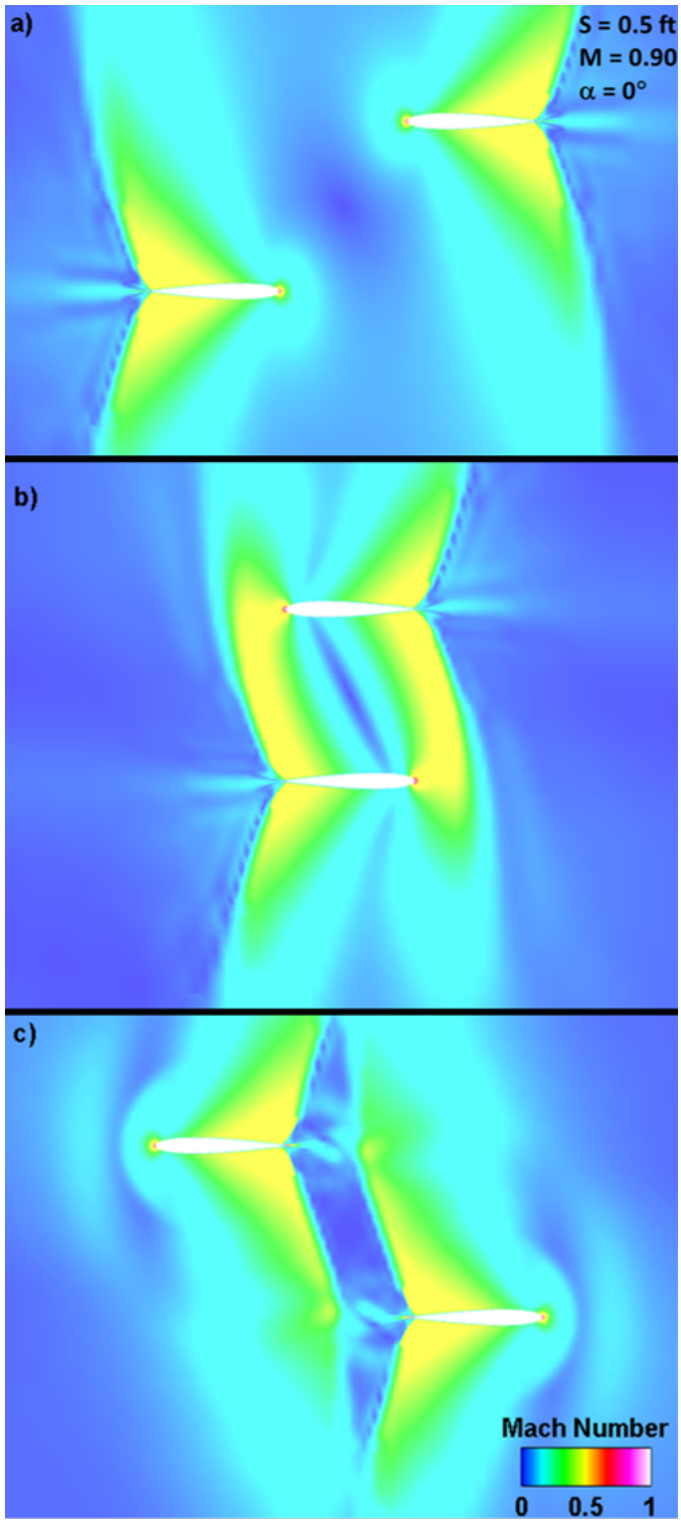

FIGURE 17. FLOW FIELD MACH NUMBER DISTRIBUTION CALCULATIONS FOR NACA 0012 AIRFOILS AT M = 0.90, S = 0.5 FT, AND $\alpha = 0°$ a) BEFORE, b) AT, AND c) AFTER CROSSING.